

# Trials Factor for Semi-Supervised NN Classifiers in Searches for Narrow Resonances at the LHC

Benjamin Lieberman<sup>1,2\*</sup>, Andreas Crivellin<sup>3,4</sup>, Salah-Eddine Dahbi<sup>1</sup>, Finn Stevenson<sup>1,2</sup>, Nidhi Tripathi<sup>1,2</sup>, Mukesh Kumar<sup>1</sup> and Bruce Mellado<sup>1,2</sup>

<sup>1</sup> School of Physics and Institute for Collider Particle Physics, University of the Witwatersrand, Johannesburg, South Africa.

<sup>2</sup> iThemba LABS, National Research Foundation, Somerset West, South Africa.

<sup>3</sup> Physik-Institut, Universitat Zurich, Winterthurerstrasse 190, CH-8057 Zurich, Switzerland.

<sup>4</sup> Paul Scherrer Institut, CH-5232 Villigen PSI, Switzerland.

\* benjamin.lieberman@cern.ch

April 12, 2024

## Abstract

To mitigate the model dependencies of searches for new narrow resonances at the Large Hadron Collider (LHC), semi-supervised Neural Networks (NNs) can be used. Unlike fully supervised classifiers these models introduce an additional look-elsewhere effect in the process of optimising thresholds on the response distribution. We perform a frequentist study to quantify this effect, in the form of a trials factor. As an example, we consider simulated  $Z\gamma$  data to perform narrow resonance searches using semi-supervised NN classifiers. The results from this analysis provide substantiation that the look-elsewhere effect induced by the semi-supervised NN is under control.

## Contents

<b>1</b>	<b>Introduction</b>	<b>2</b>
<b>2</b>	<b>Simulated Dataset</b>	<b>4</b>
2.1	Monte Carlo Simulation	4
2.2	Data sampling and generation	5
<b>3</b>	<b>Methodology</b>	<b>6</b>
3.1	Semi-supervised neural network	7
3.2	Background rejection scan	8
3.3	Significance calculation for a resonance in the invariant mass distributions	8
<b>4</b>	<b>Results and Discussion</b>	<b>9</b>
<b>5</b>	<b>Conclusion</b>	<b>11</b>
<b>A</b>	<b>Example Plots of Fits to Signal and Background</b>	<b>13</b>
<b>B</b>	<b>Machine Learning Data Generation</b>	<b>13</b>
B.1	Kernel Density Estimator (KDE)	13
B.2	Wasserstein Generative Adversarial Network (WGAN)	14
B.3	Variational Auto-encoder + Discriminator (VAE+D)	15

## 1 Introduction

The discovery of the Brout-Englert-Higgs boson [1–4], a scalar resonance, by the ATLAS [5] and CMS [6] collaborations in 2012, marked a significant milestone, completing the particle spectrum of the Standard Model (SM). The endeavour to unearth beyond the SM (BSM) physics hinges significantly on the searches for new particles in the form of narrow resonances. However, the lack of confirmed signals in inclusive or benchmark analyses implies that potential new resonances concealed within the data are likely to be subtle. Such subtlety could be the result of complex production and decay topologies that evade coverage by standard analyses (for a review of the subject see Ref. [7]). Consequently, BSM resonances might have evaded detection, lurking unnoticed within uncharted or inadequately explored regions of the phase space.

Machine Learning has the substantial promise of addressing this challenge. It has already demonstrated considerable effectiveness in probing areas of special interest, exemplified by the detection of the SM Higgs boson. These “standard” fully supervised techniques, which rely on the knowledge of event-by-event truth-level information, called “labels”, can falter if the manifestation of BSM physics diverges from the model used as a reference. This means that if the simulated data on which these models are trained is too specific or flawed, due to bias or insufficient truth-level information, the model will learn these artifacts of the simulation and might not recognise inherent signals. To reduce this model dependency, weakly supervised methods can be used [8–10] which do not enforce labels for the signal events.

The classification without labels (CWoLa) study, presented by the ATLAS collaboration, introduces weak learning techniques to reduce the dependency of the recognition mechanism on simulated data [11]. The study uses mixed samples (combining signal and background events in each sample) to train binary classification models. It reveals that weakly supervised models can classify signal events with success comparable to the fully supervised method [12–15]. Variations of the weakly supervised method have been successfully implemented for resonance detection in Refs. [16–19]. A further advantage of the weakly supervised method is shown to be its ability to be trained on impure<sup>1</sup> mixed samples [20], or directly on data, reducing the need for simulation. Research on the use of weak supervision in particle physics has been extended to include multi-model classifiers [21], graph neural networks [22], with the potential inclusion of transfer learning [23]. Finally, the viability of the methodologies for narrow resonance searches was studied in Refs. [16, 17] and a review of weak supervision was presented in Ref. [24].

This weakly or semi-supervised method can be adapted to use partial labelling, with a labelled background sample and an unlabelled mixed (signal and background) sample. This methodology allows the classifier to learn to distinguish background events from signal events by being trained on a background-only sample of simulated events. By subtracting the learned background events from the mixed sample, one is left only with the signal events of interest. The mixed sample can therefore consist of actual LHC data, allowing for a model-independent extraction of signal events. This semi-supervised technique, implemented via a side-band analysis, is therefore able to reduce model dependency and detect BSM physics with topological

---

<sup>1</sup>An impure sample refers to a dataset containing not only the signal and background of interest, but also additional signals.

variations between the possible signal and side-band regions [25].

When conducting any resonance search, it is crucial to take into account the look-elsewhere effect to arrive at a statistically meaningful result, i.e. significance for an excess. This effect refers to the increased probability of finding apparent signals (that are actually statistical fluctuations) when searching over an extended parameter range, usually mass. When using semi-supervised classifiers, an additional look-elsewhere effect is introduced. This is due to the fact that the signal sample, used for training, is not predefined like in the fully supervised method and a scan must be performed on the response distribution to determine the optimal threshold cut. This scan of the response distribution introduces an additional look-elsewhere effect that can manifest itself as "fake signals" which can significantly distort resonance patterns and influence their interpretations [26]. Hence, it is imperative to evaluate the probability of fake signals produced in the implementation of semi-supervised classifiers and expose it in the form of a trials factor. Importantly, this trials factor has to be included on top of the trials factor taking into account the probability of statistical fluctuations over e.g. an extended mass range, and thus occurs even if the mass of the new resonance is fixed (known).

In general, model-independent searches for narrow resonances are of great interest. In recent years the field of particle physics has experienced a growing plethora of anomalous experimental results (for recent reviews see Refs. [27,28]). Many of them are statistically significant, continue to grow, and remain unexplained by state-of-the-art SM calculations. While some anomalies might eventually find resolution within the SM, persisting ones could contain signs of new physics and may serve as a guide to model building and experimental searches. Of particular relevance to this paper are the multi-lepton anomalies at the LHC [29–38]. These comprise excesses in final states with charged leptons (electrons and muons), missing energy (with and without hadronic and  $b$ -jets), in processes that have SM Higgs-like topologies. They can be explained by introducing (at least) three additional scalar fields,  $H$  and  $S$ , and  $S'$  [39,40]. The scalar  $H$  has a mass in the ballpark of 270 GeV, while  $S(S')$  have masses close to that of the SM Higgs. From the di-lepton component of the multi-lepton anomalies, and assuming  $S \rightarrow W^+W^- \rightarrow \ell\ell\nu\nu$ ,  $\ell = e, \mu$ , the mass of  $S$  was determined to be  $m_S = 150 \pm 5$  GeV [31], which was later confirmed in Refs. [33,38]. The first indication of a narrow resonance within this mass range of the di-photon spectrum was reported at  $m_S = 151.5$  GeV in Ref. [41] and further corroborated with more data in Ref. [42].<sup>2</sup> Furthermore, an excess around 95 GeV, denoted  $S'$  (which acts as the main source of  $b$  quarks), has been observed [37,42,44–47]. This provides a compelling reason to seek Higgs-like resonances near the electroweak (EW) scale, an area where SM backgrounds are quite significant. The use of topological constraints through semi-supervision could be crucial in this context, as they help to dampen the impact of these backgrounds, while reducing model dependencies in the search.

In this paper, we focus on the  $S(151.5)$  candidate which is expected to be produced in associated production, i.e. jointly with a litany of different final states, and consider a simulated  $Z\gamma$  dataset. For this we present the methodology and result of a frequentist approach to estimate the look-elsewhere effect introduced in the training and implementation of semi-supervised neural network (NN) classifiers. The frequentist approach involves repeating a pseudo-experiment many thousands of times, before using the distribution of results to quantify the probability of observed outcomes. Motivated by the multi-lepton anomalies and the excess around 150 GeV, each pseudo-experiment is designed to expose the significance of fake signal, found around this mass, after training the model and extracting events from its response. Additionally, in order to obtain a sufficient quantity of simulated training data, to implement the frequentist study, an evaluation of ML-based data generators for scaling and sampling HEP datasets is presented.

<sup>2</sup>At the time of the manuscript submission new excesses at the same mass have been reported in Ref. [43].

## 2 Simulated Dataset

Our objective is to investigate the likelihood that a semi-supervised NN produces a false signal. This involves determining the probability that, in the absence of any actual signal events, the NN still identifies or creates resonance signatures. Therefore, we only need to consider and simulate the background events for the corresponding search. However, since we need many pseudo-experiments for a frequentist study, we will not only rely on Monte Carlo (MC) methods for generating this background but also use machine learning tools for scaling the MC events in a computationally efficient way.

### 2.1 Monte Carlo Simulation

The dominant background, for our example search for the  $S(150\text{ GeV}) \rightarrow Z\gamma$  decay, is the production of a prompt photon and a  $Z$  boson [48], accounting for more than 92% of the total background [49].<sup>3</sup> A sample of 110'000 SM  $Z\gamma$  MC events are simulated using MadGraph5 aMC@NLO 2.6.7 with Next-to-Leading Order accuracy in QCD [50]. The parton showering and hadronisation were simulated with PYTHIA 8.2 [51] using ATLAS A14 event tuning and NNPDF2.3 next-to-leading order simulation with a leading-order parton distribution function set [52]. Events were processed with Delphes 3 [53], which provides an approximate fast simulation of the ATLAS detector. A set of generator-level cuts were applied, where the transverse momentum of the photons was required to be greater than 25 GeV. Hadronic jets were reconstructed using the anti- $k_t$  algorithm [54] with the radius parameter,  $R = 0.4$ , as implemented in the FastJet 3.2.2 [55] package, and jets with  $p_T > 30\text{ GeV}$  and  $|\eta| < 4.7$  are considered. In addition, jets originating from bottom quarks are identified as  $b$ -jets with  $b$ -tagging algorithm [56]. Reconstructed jets overlapping with photons, electrons or muons in a cone of size  $R = 0.4$  are removed. Electrons and muons are required to have  $p_T > 25\text{ GeV}$  and  $|\eta| < 2.5$ .

The observables to be used as kinematic features in our study are:

- The  $Z\gamma$  invariant mass ( $m_{\ell\ell\gamma}$ ).
- Missing transverse energy ( $E_T^{\text{miss}}$ ).
- Missing transverse energy azimuthal angle ( $\Phi_{E_T^{\text{miss}}}$ ).
- The distance between the two leptons in the  $\eta - \phi$  space ( $\Delta R_{\ell\ell}$ <sup>4</sup>).
- The difference between the azimuthal angle of the two leptons ( $\Delta\Phi_{\ell\ell}$ ).
- The difference between the azimuthal angle of the missing transverse energy and  $Z\gamma$  system ( $\Delta\Phi(E_T^{\text{miss}}, Z\gamma)$ ).
- The number of jets ( $N_j$ ), and the number of central jets ( $N_{cj}$ ).

The feature distributions of the MC dataset are shown in Figure 1. All observables, excluding  $m_{\ell\ell\gamma}$ , are used as inputs for the NN classifier. The  $m_{\ell\ell\gamma}$  distribution, and any features with high correlation with it, cannot be used to train the NN due to the fact that the training samples, side-band and mass window, are defined on this mass.

<sup>3</sup>A secondary contribution comes from the production of  $Z$  bosons in association with jets ( $Z$ +jets), with one jet misidentified as a photon. The  $Z$ +jets background is not considered in this study as its contribution is derived from real data at the LHC.

<sup>4</sup>The distance  $\Delta R$  between two leptons in the  $\eta - \phi$  space is defined as  $\Delta R = \sqrt{(\Delta\eta_{\ell\ell})^2 + (\Delta\phi_{\ell\ell})^2}$ .

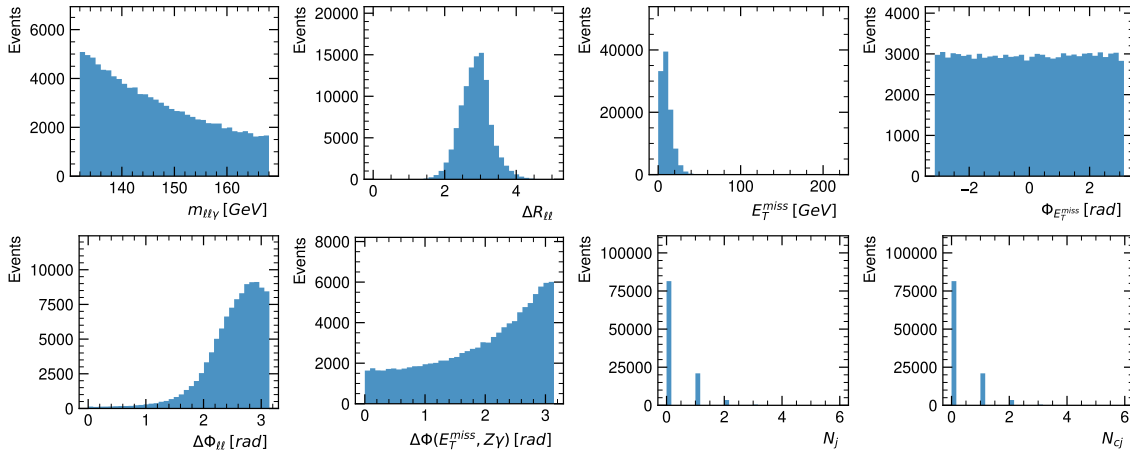


Figure 1: Selected kinematic distributions of the MC generated  $Z\gamma$  background dataset consisting of 110'000 events.

## 2.2 Data sampling and generation

Frequentist studies require a sufficient number of repetitions of an experiment to have statistically meaningful results. For each iteration of the pseudo-experiment, a sample of 80'000 events is used to train and evaluate the NN classifier, in order for the results not to be limited by the MC statistics. However, repeatedly generating these samples of events with pure MC methods would require substantial computational resources and time [57]. Fortunately, machine learning-based data generators have recently emerged as a novel and powerful tool for generating and scaling data samples [58, 59]. These advanced algorithms leverage the potential of ML and deep learning to create realistic, high-quality simulated datasets. Such data generators utilize various architectures, most notably Generative Adversarial Networks (GANs) and Variational Autoencoders (VAEs), each demonstrating unique capabilities and potential use-cases in particle physics.

To generate a sufficient quantity of high-quality data for this frequentist analysis, the three best-performing methods were found to be the Wasserstein GAN (WGAN), the VAE with an additional discriminator (VAE+D), and the Kernel Density Estimation (KDE). The model architectures, training mechanisms and resultant plots, for each method, are presented in Appendix B. The models are each trained and evaluated on the previously generated  $Z\gamma$  MC dataset. The quality of the data produced using each method is evaluated with the following metrics to compare them to the MC training data. This is firstly implemented in terms of the feature distributions, using the bin-wise relative difference and Kolmogorov-Smirnov score [60]. Furthermore, the events feature-wise correlation is evaluated using the Spearman correlation coefficient [61] and the absolute difference between the training and generated correlations, to expose the extent to which the generated events reflect true physics. To evaluate the model's ability to produce many samples of sufficient quality, the mean evaluation metric results for 500 generated samples (of 80'000 events each), using the different methods, are summarised in Table 1.

The result of comparing the different data generation methods demonstrates that the WGAN, VAE+D and KDE are each able to simulate physics events of excellent quality. The best-performing model to generate data for the frequentist study is shown to be the KDE method. An example set of pseudo-experiment data generated by the KDE is presented in the form of feature distributions, in Figure 2, and feature correlations, in Figure 3.

Table 1: Comparative evaluation of the WGAN, VAE+D and KDE data generation techniques. This table presents the mean and standard deviation of evaluation metric results for each model, based on 500 generated  $Z\gamma$  samples, to assess their performance.

Evaluation Metric	WGAN	VAE+D	KDE
Relative difference	$2.67 \times 10^{-3}$ ( $\pm 3.1 \times 10^{-5}$ )	$4.42 \times 10^{-3}$ ( $\pm 2.2 \times 10^{-5}$ )	$3.21 \times 10^{-4}$ ( $\pm 1.6 \times 10^{-5}$ )
Kolmogorov-Smirnov score	$2.67 \times 10^{-2}$ ( $\pm 2.89 \times 10^{-4}$ )	$5.55 \times 10^{-2}$ ( $\pm 3.04 \times 10^{-4}$ )	$4.50 \times 10^{-2}$ ( $\pm 2.18 \times 10^{-4}$ )
Spearman correlation coefficient	$6.96 \times 10^{-1}$ ( $\pm 5.99 \times 10^{-3}$ )	$6.23 \times 10^{-1}$ ( $\pm 7.07 \times 10^{-3}$ )	$9.38 \times 10^{-1}$ ( $\pm 1.37 \times 10^{-2}$ )
Spearman p-value	$3.43 \times 10^{-23}$ ( $\pm 5.19 \times 10^{-23}$ )	$1.38 \times 10^{-17}$ ( $\pm 1.67 \times 10^{-17}$ )	$8.95 \times 10^{-54}$ ( $\pm 1.84 \times 10^{-52}$ )
Correlation difference	$2.14 \times 10^{-2}$ ( $\pm 2.84 \times 10^{-4}$ )	$2.62 \times 10^{-2}$ ( $\pm 3.27 \times 10^{-4}$ )	$2.47 \times 10^{-3}$ ( $\pm 2.11 \times 10^{-4}$ )

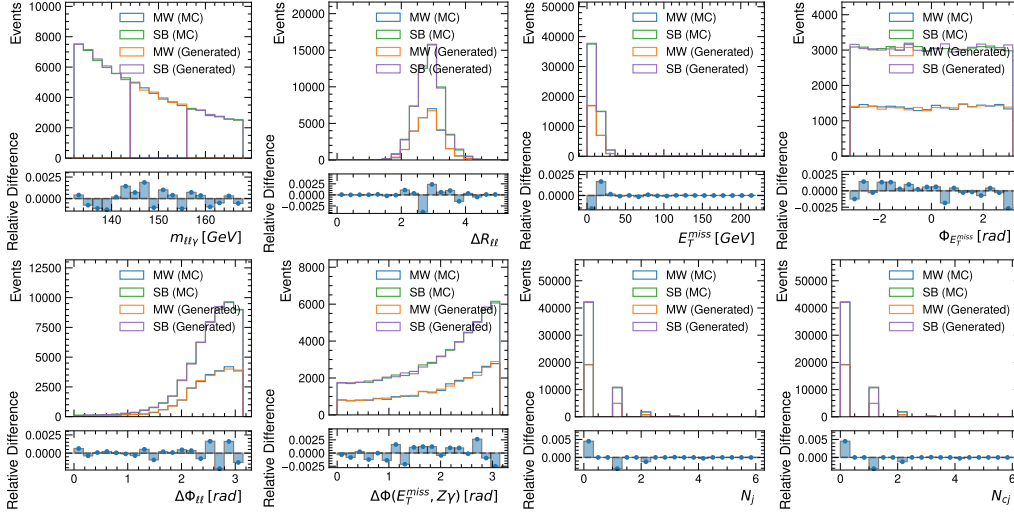


Figure 2: Feature distribution comparison between the MC and KDE generated events, for one example of the pseudo-experiments. Each feature distribution is divided into events in the mass-window (MW) and side-band (SB).

### 3 Methodology

Machine learning classifiers use the underlying patterns within the data to obtain a designated output. In particle physics, this process has the potential to introduce fake signals. This means that using a NN to observe an excess might be more probable than what is expected based on statistical fluctuations only. This can influence the statistical significance of any discovery of a narrow resonance. To evaluate the propensity of semi-supervised NN classifiers to introduce these fake signals, a frequentist methodology is used here.

A frequentist study evaluates probabilities by repeating a pseudo-experiment many times. The pseudo-experiment in this study consists of training and evaluating a semi-supervised NN

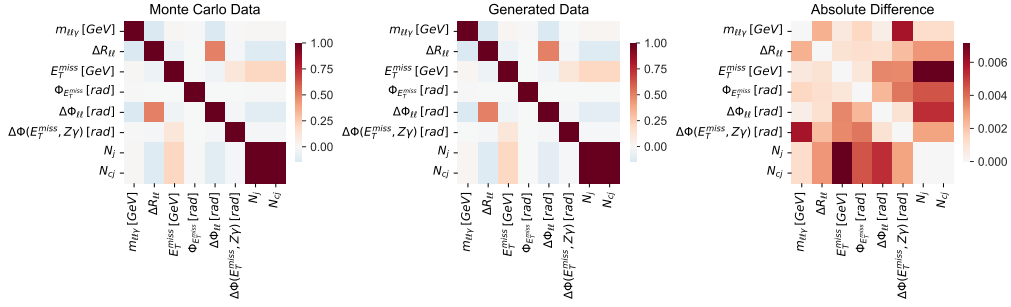


Figure 3: Feature correlation comparison between the MC and KDE generated events, for an example pseudo-experiment. Left: feature correlation of MC training dataset. Middle: feature correlation of KDE generated dataset. Right: the absolute difference between the feature correlations of the MC and KDE generated datasets.

classifier on samples of SM  $Z\gamma$  KDE generated events. The steps of the pseudo-experiment, shown in Figure 4, include data sampling, NN training, background rejection scans and the calculation of the local signal significance for an excess in the signal region. Each of these components are described in detail in the following sections.

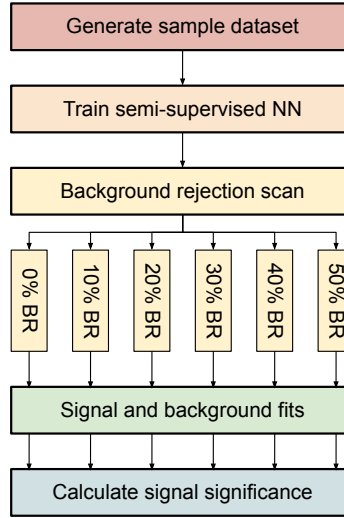


Figure 4: Diagram illustrating the methodology for a pseudo-experiment to assess possible trails factors when using a semi-supervised NN in the search for a narrow resonance. The process starts with the generation of a sample dataset, followed by the training of the semi-supervised NN. Subsequent stages include a background rejection scan to extract local samples from the NN response, fitting signal and background models to each local sample, and finally the computation of the signal significance.

### 3.1 Semi-supervised neural network

The Neural Network classifier used in this study is implemented using the PyTorch framework [62]. The model architecture consists of an input layer, three hidden layers and an output layer. The input layer has seven neurons, each corresponding to one of the selected

input features, described in Section 2. The number of neurons in each of the hidden layers are 26, 26 and 13, respectively. The hidden layers each use the hyperbolic tangent activation function,  $Tanh$  [63]. The output layer consists of one neuron and is activated by a  $Sigmoid$  function, constraining the output response to a value between zero and one.

For each iteration of the pseudo-experiment, the NN model is trained independently, on the corresponding data sample, for 50 epochs using the Adam [64] optimiser, a learning rate of  $10^{-3}$ , and a batch size of 256 events. The training uses a background sample and a mixed sample. The background sample consists of the events in the side-band regions which are labelled as background (0). The mixed sample is made up of events within the mass window of interest, and are labelled as signal (1). As only  $Z\gamma$  data intended as a background is used, no actual signal events are present in the mixed sample, therefore the training samples should be indistinguishable to the NN apart from statistical fluctuations. This means that the NN should not be able to discriminate between the samples to the extent that any excess of signal events found in the signal region can be considered a fake signal.

### 3.2 Background rejection scan

Once trained, the NN model is used to infer a response value for each event, where values tending to zero indicate background and events tending to one indicate signal. In the semi-supervised context, the extraction of signal events using the NN response can be understood as the rejection of background events. By rejecting background events, which are events with a response tending to zero, a sample of signal events is left. The optimal background rejection cut on the response distribution must therefore be determined to remove as many background events as possible from the sample. To simulate the process of optimising the background rejection cut, to maximise the purity of the signal sample, a scan of cuts to the model's response distribution is implemented. When conducting a statistical analysis in which a scan is performed, the extent of the corresponding look-elsewhere effects must be considered.

To understand this additional look-elsewhere effect, the background rejection scan is used to extract samples of events with increasing amounts of rejected background events. The amount of background events rejected in each sample is selected to be 0, 10, 20, 30, 40 and 50 percent of the total events respectively. As there are no signal events present to classify, the defined cuts provide samples of events with increasing influence of background rejection, while maintaining at least half of the event statistics. The six batches of events extracted, for each background rejection, can therefore each be considered a local analysis sample. For a given pseudo-experiment, each local sample will be fitted to measure a local resultant signal significance, revealing any fake signals in the sample. To this end, each local sample is mapped to its respective invariant mass for further analysis.

### 3.3 Significance calculation for a resonance in the invariant mass distributions

In this analysis, the resonant anomaly detection search strategy is used to discover evidence for BSM physics. The new physics signal is expected to originate from a decay of a new particle,  $S$ , in the form of a resonance in the corresponding invariant mass. The investigation therefore involves searching for an excess with respect to the continuous SM background. Since we want to examine the probability of a fake signal, we define a signal region (or mass window) in the invariant mass,  $m_{\ell\ell\gamma}$ , where an excess of signal events can be observed. We select a fixed center of mass of  $m_{\ell\ell\gamma} \approx 150$  GeV, motivated by the corresponding excess [31, 38, 41, 42]. The background (or side-band) region is defined as the mass range surrounding the signal region where only SM background events are expected. The signal (mass-window) range is defined as  $144 \leq m_{\ell\ell\gamma} \leq 156$  GeV and the background (side-band) range as  $132 < m_{\ell\ell\gamma} < 168$  GeV excluding the mass-window.



The invariant mass distribution of each background rejection sample is used to calculate the significance of a local excess, if present, in the prescribed mass window. To determine the extent of any signal excesses, a background-only hypothesis is used. The background is defined using the functional form expressed in Equation 1 in Ref. [41]:

$$f(\epsilon_m) = (1 - \epsilon_m)^{c_0} \cdot \epsilon_m^{c_1 + c_2 \cdot \log(\epsilon_m)}, \quad (1)$$

where  $c_0$ ,  $c_1$  and  $c_2$  are fit parameters and  $\epsilon_m$  is the invariant mass,  $m_{\ell\ell\gamma}$ , divided by the center of mass energy, i.e. 13 TeV. Excesses of signal events within the mass window are captured using a Gaussian function, Equation 2:

$$g(m) = c_s \cdot e^{-\frac{(m - \mu_s)^2}{2 \cdot \sigma_s^2}} \quad (2)$$

where  $m$  is the invariant mass,  $c_s$  is the parameter measuring the height of the peak,  $\mu_s$  is the position of the center of the peak, and  $\sigma_s$  is the search resolution. In this analysis, the  $\mu_s$  is fixed at 150 GeV and  $\sigma_s$  is set to the search resolution of 2.4 GeV [49].

The probability density function, composed of the signal and background functions, is minimised using the negative log-likelihood, allowing any signal events to be captured by the Gaussian function. By integrating over the mass range for the signal and background fits, the number of signal and background events can be extracted. Using the number of signal and background events, the local significance,  $Z$ , can be calculated as

$$Z = \sqrt{2 \cdot \left( (N_s + N_b) \cdot \log \left( 1 + \frac{N_s}{N_b} \right) - N_s \right)}, \quad (3)$$

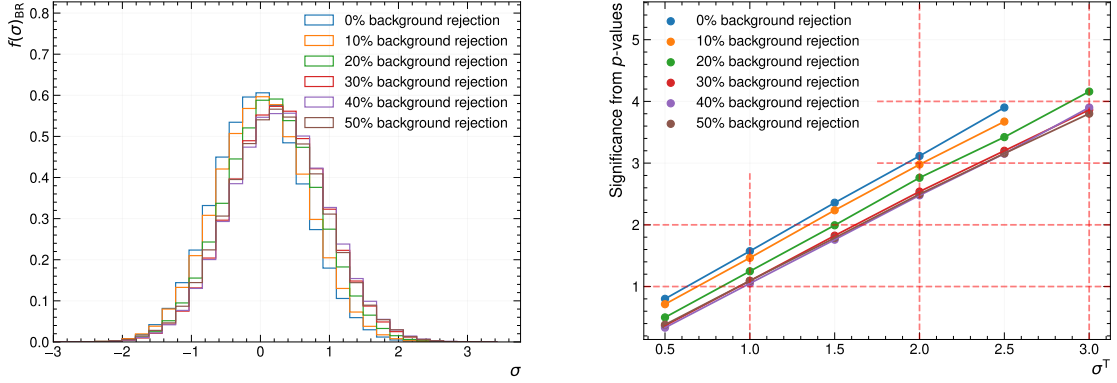
where  $N_s$  and  $N_b$  are the number of signal and background events respectively. Each pseudo-experiment will therefore produce six local significance values, reflecting each background rejection sample. An example of the signal and background fits for a single iteration of the pseudo-experiment are shown in Appendix A, Figure 8.

## 4 Results and Discussion

We use a frequentist approach to explore the size of the additional look-elsewhere effect originating from the implementation of the semi-supervised classifier. To this end, the pseudo-experiment presented in Section 3 is repeated 125'000 times to obtain the necessary statistics. This means that for each pseudo-experiment the KDE model, pre-trained on the  $Z\gamma$  MC-generated dataset of 110'000 events, is used to generate a new sample of 80'000 statistically independent events. These events are then used to train the semi-supervised NN. Then, the event samples for the background rejection cuts of 0%, 10%, 20%, 30%, 40% and 50% are extracted via the NN response distribution. The invariant  $Z\gamma$  mass distributions of these samples are then used to calculate the significance for the existence of a narrow resonance at 150 GeV. Therefore, each pseudo-experiment will produce six (local) significance values, corresponding to each of the background rejection thresholds.

This methodology, similar to mass scans in high-energy physics, segments our analysis through the use of background rejection (BR) samples, where each threshold acts as a local category. Each category, however, is not statistically independent as the events in each sample overlap. This approach facilitates an examination of the impact of background rejection levels on our results, enabling a nuanced understanding of their influence on our findings. The probability density functions (PDF) of the significances for the six different background rejection cuts ( $f(\sigma)_{\text{BR}}$ ) are shown in Figure 5a. Note that these distributions have approximately a

Gaussian shape, however with a standard deviation between 0.65 and 0.71. This decrease in variance w.r.t. the standard Gaussian is due to the constraints within the resonance fit imposed a priori via the shape of the resonance and the side-bands definitions. Note that the peak of the PDFs shifts to the right with an increasing background rejection cut. Such a shift emerges from the interplay between signal and background modelling, amplified by the diminishing event counts in samples subjected to higher background rejection cuts.



(a) PDFs of the significance for an excess at 150 GeV obtained from the pseudo-experiments for each (local) background rejection cut.

(b) Positive local background rejection  $p$ -values (converted to significance) as compared to significance thresholds.

Figure 5: PDFs and comparison to a standard Gaussian for the local samples, i.e. the different background rejection cuts.

To further interpret these results and quantify the deviations from a Gaussian shape, the probability of getting a local significance of up to  $1\sigma$ ,  $2\sigma$  and  $3\sigma$  can be calculated for each BR cut sample. For this, we consider only positive values of the significances for an excess at 150 GeV, as only they can reflect instances where a fake signal is generated. The corresponding normalised probability density function is

$$f^+(\sigma)_{\text{BR}} = \frac{f(\sigma)_{\text{BR}}}{\int_0^{\infty} f(\sigma) d\sigma}, \quad \text{for } \sigma > 0, \quad (4)$$

where BR is a label indicating the local background rejection cut. We then compute the probability that, for each background reject cut, a significance of up-to a value  $\sigma^T = 1\sigma$ ,  $2\sigma$  and  $3\sigma$  is obtained via the cumulative distribution function (CDF):

$$F(\sigma^T)_{\text{BR}} = \int_0^{\sigma^T} f^+(\sigma)_{\text{BR}} d\sigma. \quad (5)$$

Therefore, the corresponding  $p$ -values calculated as  $1 - F(\sigma^T)_{\text{BR}}$ , quantify the probability of detecting an excess of up-to  $\sigma^T$ . These  $p$ -values can be converted to significance, before being directly compared to  $\sigma^T$ , corresponding to if the distribution were normally distributed. This relationship is shown in Figure 5b, where one can see that the local samples conform to a large degree with expected probabilities from a Gaussian distribution. Only at higher significance thresholds above  $\approx 2.5\sigma$  slight deviations from the diagonal are seen. It is also shown that for background rejection cuts of 0% and 10%, no  $3\sigma$  significance excesses were found during the 125'000 iterations.

To understand the extent of additional look-elsewhere effect introduced, the 0% BR sample can be used as a baseline. This inclusive sample contains all the events classified by the NN

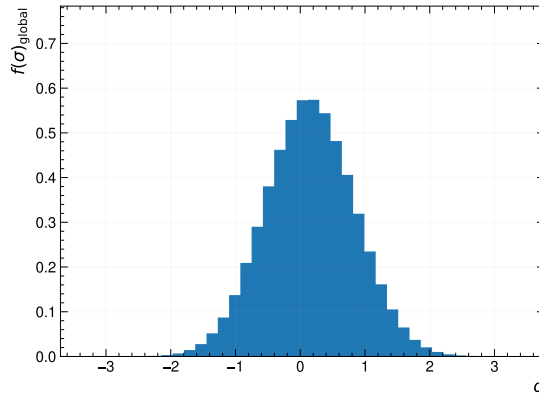


Figure 6: Probability density distribution of the significance from the global sample, i.e. averaged over the different background rejection cuts.

without any cuts applied, and therefore provides a sample unaffected by the influence of the classifier and its response scan. The additional look-elsewhere effect can thus be revealed through a comparison of the samples that include the influence of the NN, from response cuts, to the inclusive baseline.

The “global” PDF

$$f(\sigma)_{\text{global}} = \sum_{i=1}^6 f(\sigma)_i, \quad (6)$$

where  $i$  represents the different background rejection cuts, is used to the average of all background rejection categories. It is shown in Figure 6 from where one can see that it approximates a Gaussian distribution with a standard deviation of 0.69 centred around a mean of 0.15. The corresponding global  $p$ -value is calculated as

$$p_{\text{global}}(\sigma^T) = 1 - \int_0^{+\sigma^T} f^+(\sigma')_{\text{global}} d\sigma', \quad (7)$$

where  $f^+$  is defined analogously to Eq. (4).

The comparison of the  $p$ -values from the different BR cuts sample and the corresponding global PDF are compared to the 0% BR cut  $p$ -value to quantify additional look-elsewhere effects. This means a trials factor is defined as the ratio of these  $p$ -values, as shown in Figure 7. For lower significances, up to approximately  $1.5\sigma$ , the trials factor is close to 1, implying minimal inflation in the observed significance. However, at higher significances, of greater than  $2\sigma$  thresholds, the trials factor displays elevations, indicating an inflation of significance due to the NN procedure.

Therefore, despite the inherent challenges for resonant searches using weak supervision, the depicted results demonstrate the efficacy of semi-supervised techniques and their ability to maintain additional look-elsewhere effects within acceptable bounds. This means that the false signals introduced by the NN are under control.

## 5 Conclusion

In this article we critically evaluated the efficacy of semi-supervised NN classifiers within the realm of narrow resonance searches in high-energy physics, gauging their tendency to produce additional look-elsewhere effects in the form of fake signals related to the selection of

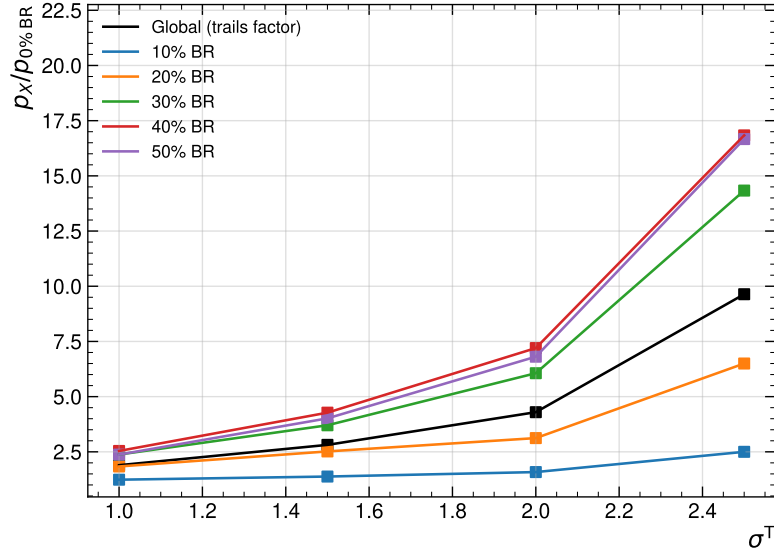


Figure 7: The ratio  $p_X/p_{0\%BR}$  for  $X = 10\%, 20\%, 30\%, 40\%, 50\%$  BR cuts and  $p_{\text{global}}/p_{0\%BR}$ , corresponding to the trails factor, as a function of the significance threshold,  $\sigma^T$ .

the background rejection cut. For this, we first generated the  $Z\gamma$  MC dataset introduced in Section 2.1, which is then used to train and optimise the WGAN, VAE+D and KDE generative models. The optimised models were compared, revealing their ability to generate high-quality HEP data based on the training set of real MC-generated data. The best-performing generative model, for the frequentist study, was found to be the KDE. The pre-trained KDE model was then selected to generate 125'000 new training datasets, of 80'000 events each. On each of these data sets, we trained the NN and considered the outcome as a pseudo-experiment for a frequentist study of the look-elsewhere effect introduced by the semi-supervised NN.

While the methodology demonstrates that this effect is very small at lower significance values, it is enhanced with decreasing  $p$ -values (see Figure 7). Despite these complexities, the difference between the baseline with 0% BR cut and  $p$ -values for higher BR cuts remain limited, showing the method's proficiency in classifying events. Critically, the results corroborate that semi-supervised NN classifiers introduce controlled fake signals, cementing their viability in HEP analyses. Therefore, this article heralds the precision and utility of semi-supervised NN classifiers for advanced HEP explorations, hinting at their pivotal role in forthcoming discoveries.

## Acknowledgements

Support of the University of the Witwatersrand as well as the South African Department of Science and Innovation through the SA-CERN program is gratefully acknowledged.

**Funding information** The work of A.C. is supported by a professorship grant from the Swiss National Science Foundation (No. PP00P21\_76884).

## A Example Plots of Fits to Signal and Background

In each of the frequentist study's pseudo-experiments, the six background rejection samples are each used to quantify the extent of fake signals in the mass window of the  $m_{\ell\ell\gamma}$  distribution. To achieve this, the  $m_{\ell\ell\gamma}$  distributions are fit with the signal and background function. Figure 8 presents the  $m_{\ell\ell\gamma}$  distribution of the six different background rejection samples, including the signal and background fits for a selected pseudo-experiment.

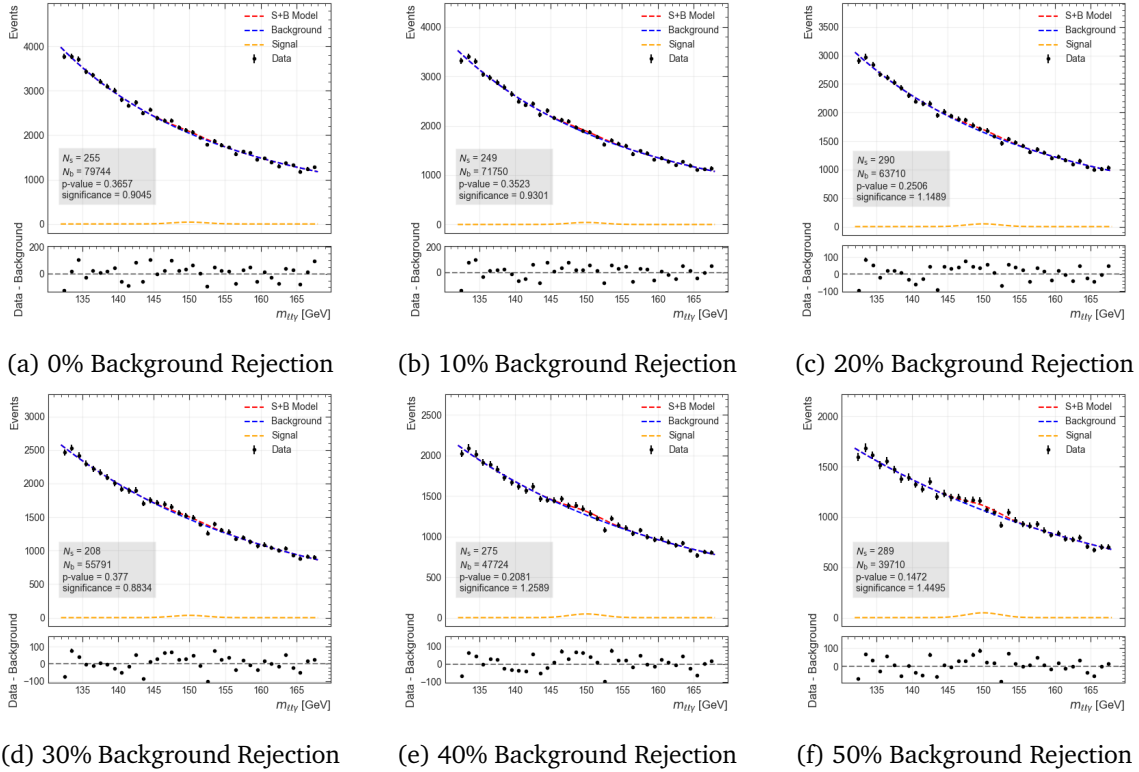


Figure 8: Signal and background fits for an example pseudo-experiment. Note that we only allow for a resonance within the signal region whose peak is centered at 150 GeV.

## B Machine Learning Data Generation

In this section, we introduce the ML-based data generation methods compared within this study. The KDE, WGAN and VAE+D methods are each introduced and their architecture and hyper-parameters are presented. This is followed by a visual demonstration of the ability of each model in the form of generated feature distributions and event-wise feature correlation.

### B.1 Kernel Density Estimator (KDE)

Kernel density estimation (KDE) is a non-parametric method for estimating the probability density function of a given random variable. The method is an unsupervised machine learning technique used to generate large samples of events that accurately reflect the statistics of real physics [65–67]. The KDE is implemented using the Scikit-learn library [68]. Through a scan of bandwidth parameters, the optimal value for this analysis was determined to be  $1 \cdot 10^{-3}$ . The resultant feature distributions and correlation plots are shown in Figures 9 and 10, respectively.

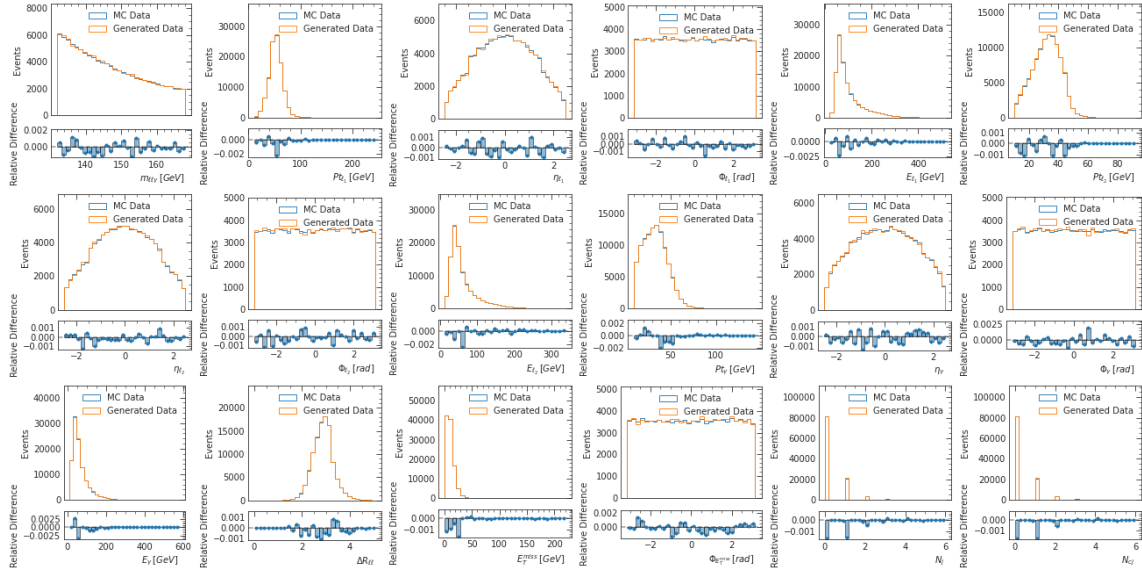


Figure 9: Feature distribution comparison between the KDE generated events and the MC events. The figures demonstrate that KDE generated feature distributions accurately reflect those of the MC dataset.

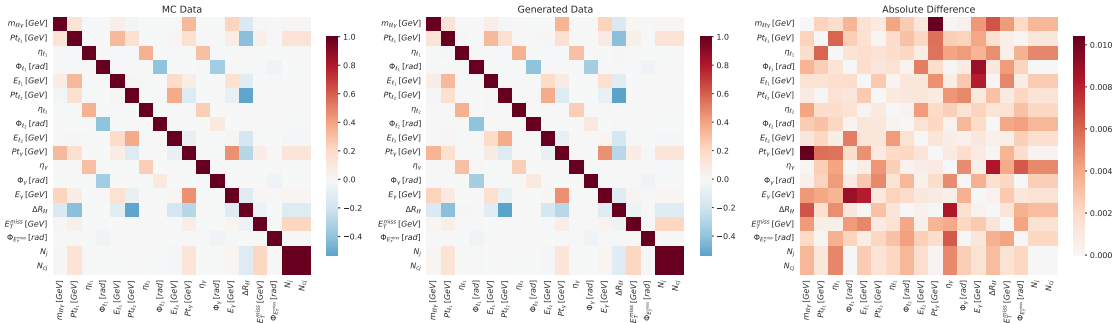


Figure 10: Feature correlation comparison between the MC and KDE generated events. Left: feature correlation of MC training dataset. Middle: feature correlation of KDE generated dataset. Right: the absolute difference between the feature correlations of the MC and KDE generated datasets. The feature correlation plots show that the maximum absolute difference between KDE generated events and MC events is 0.01.

## B.2 Wasserstein Generative Adversarial Network (WGAN)

The Generative Adversarial Network (GAN) training strategy is an interaction between two competing neural networks. The generator model,  $G$ , maps a source of noise to the desired feature space. A discriminator network receives both a generated sample and a MC data sample and is trained to distinguish between the two. The generator is trained to output realistic data, while the discriminator is simultaneously trained to distinguish the generated data from the MC data. An improved methodology of the GAN, described in Ref. [69], is the Wasserstein GAN (WGAN). This model adopts the Wasserstein distance,  $W(q, p)$ , which is defined as the minimum cost required to transform the probability distribution  $q$  into the distribution  $p$  by

moving probability mass efficiently. The discriminator is replaced in the improved model with a critic,  $C$ , and the gradients are controlled using a gradient penalty,  $GP$ . The  $GP$  penalises the normal of the critic gradients with respect to the input. The optimisation of the WGAN is a delicate interaction between the architecture and hyper-parameters of the models. The model is optimised on various combinations of architectures and hyper-parameters. The final optimised model consists of the following architectures and hyper-parameters. The Critic network consists of an input layer, three hidden layers and an output layer. The input layer has 18 nodes corresponding to the input features, the hidden layers have 256, 512 and 256 nodes, respectively, and a single neuron in the output layer. The critics neurons are activated using the ReLU activation function. The generator network consists of an input layer of 16 nodes representing latent space, four hidden layers of 256, 512, 1024, and 256 nodes respectively. The output layer consists of 18 neurons representing the input features. The generator network uses a combination of batch normalisation and ReLU as activation functions. The optimised hyper-parameters used for both the generator and critic are a learning rate, batch size, and gradient penalty constant,  $\lambda$ , of  $1 \cdot 10^{-4}$ , 256, and  $1 \cdot 10^{-3}$  respectively. To improve the ability of the critic with respect to the generator, the critic is trained five times for each time the generator is trained. The resultant generated feature distributions and correlation plots are shown in Figures 11 and 12 respectively.

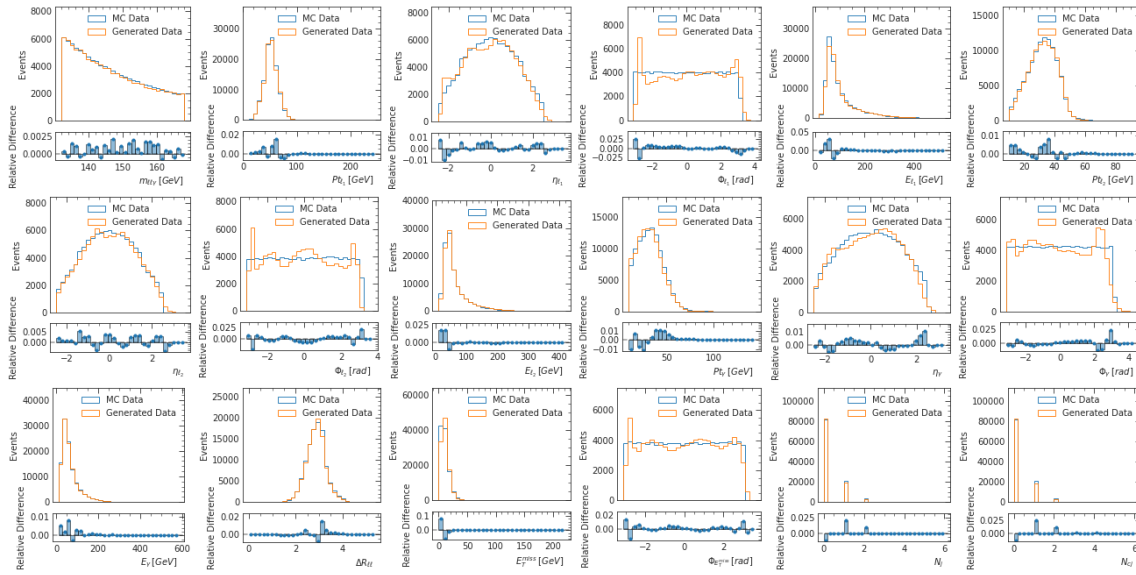


Figure 11: Feature distribution comparison between the WGAN generated events and the MC events. The figures demonstrate that the majority WGAN generated feature distributions accurately reflect those of the MC dataset.

### B.3 Variational Auto-encoder + Discriminator (VAE+D)

The Variational Autoencoder with Adversarial Training (VAE+D) is a hybrid data generation approach that combines Variational Autoencoders (VAEs) with adversarial training. VAEs are generative models used for learning latent data patterns. They encode data into a latent space and decode it back to the original space. However, VAEs can struggle with generating detailed and diverse samples. VAE+D addresses this limitation by incorporating a discriminator network, inspired by GANs. In VAE+D, the generator not only minimizes reconstruction errors but also aims to produce samples that are indistinguishable from real data according to the discriminator's judgment. The optimised VAE+D model includes the optimised encoder, decoder and discriminator networks. The encoder, decoder and discriminator networks each

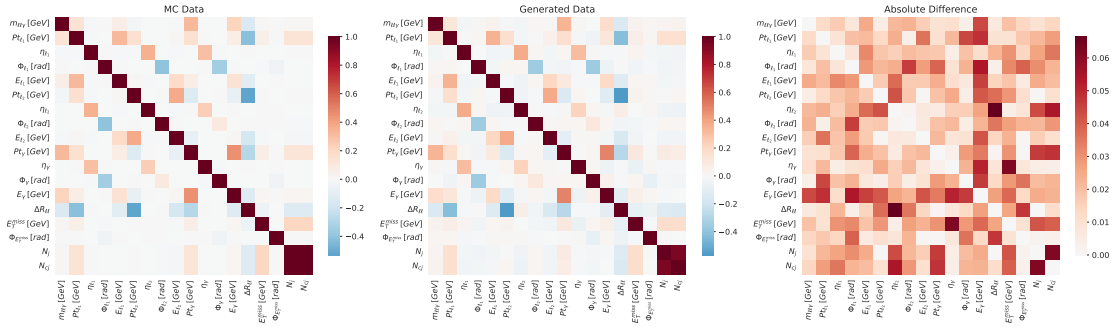


Figure 12: Feature correlation comparison between the MC and WGAN generated events. Left: feature correlation of MC training dataset. Middle: feature correlation of WGAN generated dataset. Right: the absolute difference between the feature correlations of the MC and WGAN-generated datasets. The feature correlation plots show that the maximum absolute difference between WGAN-generated events and MC events is 0.06.

have three hidden layers of 256 nodes each. The latent space input to the encoder consists of 16 nodes and the output to the decoder consists of 18 neurons representing the input features. The discriminator network has an input layer of 18 neurons reflecting the input features and a single output neuron. The eLu activation function is used to activate neurons in each network. A learning rate of  $5 \cdot 10^{-4}$ , batch size of 256 and scalar parameter  $\gamma$  of 500 are used for training. The final optimised resultant feature distributions and correlations are presented in Figures 13 and 14, respectively.

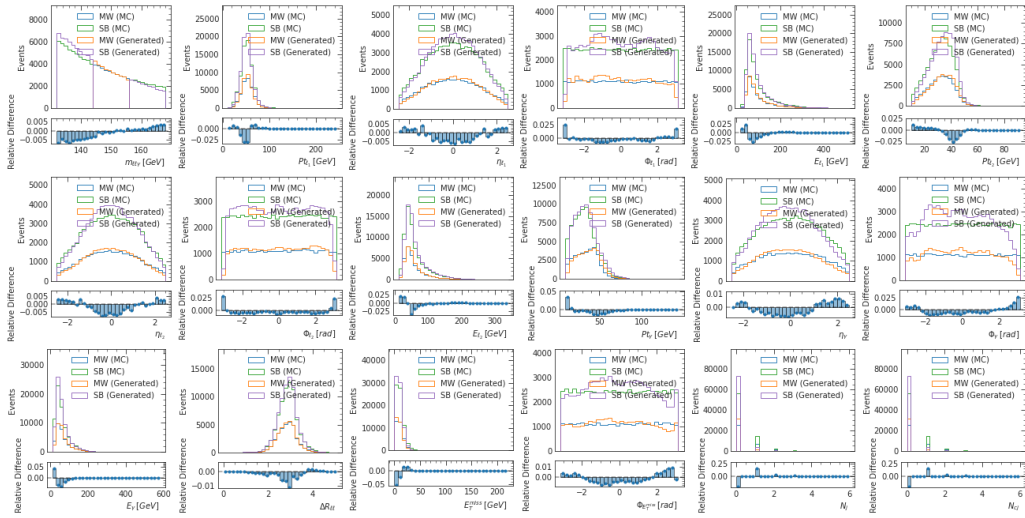


Figure 13: Feature distribution comparison between the VAE+D generated events and the MC events. Each distribution is shown in terms of the events in the mass-window (MW) and side band (SB). The figures demonstrate that the majority VAE+D generated feature distributions substantially reflect those of the MC dataset.



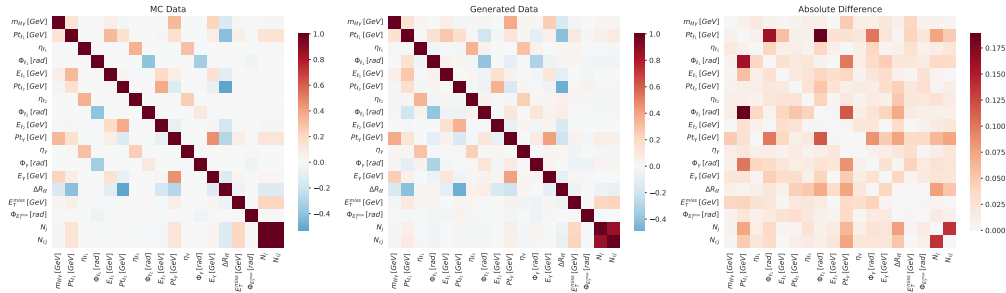


Figure 14: Feature correlation comparison between the MC and VAE+D generated events. Left: feature correlation of MC training dataset. Middle: feature correlation of VAE+D generated dataset. Right: the absolute difference between the feature correlations of the MC and VAE+D generated datasets. The feature correlation plots show that the maximum absolute difference between VAE+D generated events and MC events is 0.18.

## References

- [1] P. W. Higgs, *Broken symmetries, massless particles and gauge fields*, Phys. Lett. **12**, 132 (1964), doi:[10.1016/0031-9163\(64\)91136-9](https://doi.org/10.1016/0031-9163(64)91136-9).
- [2] F. Englert and R. Brout, *Broken symmetry and the mass of gauge vector mesons*, Phys. Rev. Lett. **13**, 321 (1964), doi:[10.1103/PhysRevLett.13.321](https://doi.org/10.1103/PhysRevLett.13.321).
- [3] F. Englert and R. Brout, *Broken symmetry and the mass of gauge vector mesons*, Phys. Rev. Lett. **13**, 321 (1964), doi:[10.1103/PhysRevLett.13.321](https://doi.org/10.1103/PhysRevLett.13.321).
- [4] P. W. Higgs, *Broken symmetries and the masses of gauge bosons*, Phys. Rev. Lett. **13**, 508 (1964), doi:[10.1103/PhysRevLett.13.508](https://doi.org/10.1103/PhysRevLett.13.508).
- [5] G. Aad, T. Abajyan, B. Abbott and J. Abdallah, *Observation of a new particle in the search for the standard model higgs boson with the atlas detector at the lhc*, Physics Letters B **716**(1), 1 (2012), doi:<https://doi.org/10.1016/j.physletb.2012.08.020>.
- [6] S. Chatrchyan, V. Khachatryan and A. Sirunyan, *Observation of a new boson at a mass of 125 gev with the cms experiment at the lhc*, Physics Letters B **716**(1), 30 (2012), doi:<https://doi.org/10.1016/j.physletb.2012.08.021>.
- [7] O. Fischer, B. Mellado, S. Antusch, E. Bagnaschi, S. Banerjee, G. Beck, B. Belfatto, M. Bellis, Z. Berezhiani, M. Blanke, B. Capdevila, K. Cheung *et al.*, *Unveiling hidden physics at the LHC*, The European Physical Journal C **82**(8) (2022), doi:[10.1140/epjc/s10052-022-10541-4](https://doi.org/10.1140/epjc/s10052-022-10541-4).
- [8] L. M. Dery, B. Nachman, F. Rubbo and A. Schwartzman, *Weakly supervised classification in high energy physics*, Journal of High Energy Physics **2017**(5) (2017), doi:[10.1007/jhep05\(2017\)145](https://doi.org/10.1007/jhep05(2017)145).
- [9] J. S. H. Lee, S. M. Lee, Y. Lee, I. Park, I. J. Watson and S. Yang, *Quark gluon jet discrimination with weakly supervised learning*, Journal of the Korean Physical Society **75**(9), 652–659 (2019), doi:[10.3938/jkps.75.652](https://doi.org/10.3938/jkps.75.652).

- [10] M. Kuusela, T. Vatanen, E. Malmi, T. Raiko, T. Aaltonen and Y. Nagai, *Semi-supervised anomaly detection – towards model-independent searches of new physics*, Journal of Physics: Conference Series **368**(1), 012032 (2012), doi:[10.1088/1742-6596/368/1/012032](https://doi.org/10.1088/1742-6596/368/1/012032).
- [11] E. M. Metodiev, B. Nachman and J. Thaler, *Classification without labels: learning from mixed samples in high energy physics*, Journal of High Energy Physics **2017**(10) (2017), doi:[10.1007/jhep10\(2017\)174](https://doi.org/10.1007/jhep10(2017)174).
- [12] J. H. Collins, K. Howe and B. Nachman, *Extending the search for new resonances with machine learning*, Physical Review D **99**(1) (2019), doi:[10.1103/physrevd.99.014038](https://doi.org/10.1103/physrevd.99.014038).
- [13] P. T. Komiske, E. M. Metodiev and J. Thaler, *An operational definition of quark and gluon jets*, Journal of High Energy Physics **2018**(11) (2018), doi:[10.1007/jhep11\(2018\)059](https://doi.org/10.1007/jhep11(2018)059).
- [14] P. T. Komiske, S. Kryhin and J. Thaler, *Disentangling quarks and gluons in cms open data*, Physical Review D **106**(9) (2022), doi:[10.1103/physrevd.106.094021](https://doi.org/10.1103/physrevd.106.094021).
- [15] T. Finke, M. Krämer, M. Lipp and A. Mück, *Boosting mono-jet searches with model-agnostic machine learning*, Journal of High Energy Physics **2022**(8) (2022), doi:[10.1007/jhep08\(2022\)015](https://doi.org/10.1007/jhep08(2022)015).
- [16] J. Collins, K. Howe and B. Nachman, *Anomaly detection for resonant new physics with machine learning*, Physical Review Letters **121**(24) (2018), doi:[10.1103/physrevlett.121.241803](https://doi.org/10.1103/physrevlett.121.241803).
- [17] G. Aad, B. Abbott, D. C. Abbott, A. Abed Abud *et al.*, *Dijet resonance search with weak supervision using  $\sqrt{s} = 13$  TeV pp collisions in the atlas detector*, Phys. Rev. Lett. **125**, 131801 (2020), doi:[10.1103/PhysRevLett.125.131801](https://doi.org/10.1103/PhysRevLett.125.131801).
- [18] D. Bardhan, Y. Kats and N. Wunch, *Searching for dark jets with displaced vertices using weakly supervised machine learning*, Physical Review D **108**(3) (2023), doi:[10.1103/physrevd.108.035036](https://doi.org/10.1103/physrevd.108.035036).
- [19] M. A. Md Ali, N. Badrud'din, H. Abdullah and F. Kemi, *Alternate methods for anomaly detection in high-energy physics via semi-supervised learning*, International Journal of Modern Physics A **35**(23), 2050131 (2020), doi:[10.1142/S0217751X20501316](https://doi.org/10.1142/S0217751X20501316), <https://doi.org/10.1142/S0217751X20501316>.
- [20] P. T. Komiske, E. M. Metodiev, B. Nachman and M. D. Schwartz, *Learning to classify from impure samples with high-dimensional data*, Physical Review D **98**(1) (2018), doi:[10.1103/physrevd.98.011502](https://doi.org/10.1103/physrevd.98.011502).
- [21] O. Amram and C. M. Suarez, *Tag n' train: a technique to train improved classifiers on unlabeled data*, Journal of High Energy Physics **2021**(1) (2021), doi:[10.1007/jhep01\(2021\)153](https://doi.org/10.1007/jhep01(2021)153).
- [22] T. Li, S. Liu, Y. Feng, G. Paspalaki, N. V. Tran, M. Liu and P. Li, *Semi-supervised graph neural networks for pileup noise removal*, The European Physical Journal C **83**(1) (2023), doi:[10.1140/epjc/s10052-022-11083-5](https://doi.org/10.1140/epjc/s10052-022-11083-5).
- [23] H. Beauchesne, Z.-E. Chen and C.-W. Chiang, *Improving the performance of weak supervision searches using transfer and meta-learning* (2023), [2312.06152](https://arxiv.org/abs/2312.06152).
- [24] T. Cohen, M. Freytsis and B. Ostdiek, *(machine) learning to do more with less*, Journal of High Energy Physics **2018**(2) (2018), doi:[10.1007/jhep02\(2018\)034](https://doi.org/10.1007/jhep02(2018)034).

- [25] S.-e. Dahbi, J. Choma, G. Mokgatitwane, X. Ruan, B. Lieberman, B. Mellado and T. Celik, *Machine learning approach for the search of resonances with topological features at the Large Hadron Collider*, *Int. J. Mod. Phys. A* **37**(03), 2150241 (2022), doi:[10.1142/S0217751X21502419](https://doi.org/10.1142/S0217751X21502419), [2011.09863](https://arxiv.org/abs/2011.09863).
- [26] P. Baldi, P. Sadowski and D. Whiteson, *Searching for exotic particles in high-energy physics with deep learning*, *Nature Communications* **5**(1) (2014), doi:[10.1038/ncomms5308](https://doi.org/10.1038/ncomms5308).
- [27] O. Fischer *et al.*, *Unveiling hidden physics at the LHC*, *Eur. Phys. J. C* **82**(8), 665 (2022), doi:[10.1140/epjc/s10052-022-10541-4](https://doi.org/10.1140/epjc/s10052-022-10541-4), [2109.06065](https://arxiv.org/abs/2109.06065).
- [28] A. Crivellin and B. Mellado, *Anomalies in Particle Physics* (2023), [2309.03870](https://arxiv.org/abs/2309.03870).
- [29] S. von Buddenbrock, N. Chakrabarty, A. S. Cornell, D. Kar, M. Kumar, T. Mandal, B. Mellado, B. Mukhopadhyaya and R. G. Reed, *The compatibility of LHC Run 1 data with a heavy scalar of mass around 270 GeV* (2015), [1506.00612](https://arxiv.org/abs/1506.00612).
- [30] S. von Buddenbrock, N. Chakrabarty, A. S. Cornell, D. Kar, M. Kumar, T. Mandal, B. Mellado, B. Mukhopadhyaya, R. G. Reed and X. Ruan, *Phenomenological signatures of additional scalar bosons at the LHC*, *Eur. Phys. J. C* **76**(10), 580 (2016), doi:[10.1140/epjc/s10052-016-4435-8](https://doi.org/10.1140/epjc/s10052-016-4435-8), [1606.01674](https://arxiv.org/abs/1606.01674).
- [31] S. von Buddenbrock, A. S. Cornell, A. Fadol, M. Kumar, B. Mellado and X. Ruan, *Multi-lepton signatures of additional scalar bosons beyond the Standard Model at the LHC*, *J. Phys. G* **45**(11), 115003 (2018), doi:[10.1088/1361-6471/aae3d6](https://doi.org/10.1088/1361-6471/aae3d6), [1711.07874](https://arxiv.org/abs/1711.07874).
- [32] S. von Buddenbrock, A. S. Cornell, E. D. Iarilala, M. Kumar, B. Mellado, X. Ruan and E. M. Shrif, *Constraints on a 2HDM with a singlet scalar and implications in the search for heavy bosons at the LHC*, *J. Phys. G* **46**(11), 115001 (2019), doi:[10.1088/1361-6471/ab3cf6](https://doi.org/10.1088/1361-6471/ab3cf6), [1809.06344](https://arxiv.org/abs/1809.06344).
- [33] S. Buddenbrock, A. S. Cornell, Y. Fang, A. Fadol Mohammed, M. Kumar, B. Mellado and K. G. Tomiwa, *The emergence of multi-lepton anomalies at the LHC and their compatibility with new physics at the EW scale*, *JHEP* **10**, 157 (2019), doi:[10.1007/JHEP10\(2019\)157](https://doi.org/10.1007/JHEP10(2019)157), [1901.05300](https://arxiv.org/abs/1901.05300).
- [34] D. Sabatta, A. S. Cornell, A. Goyal, M. Kumar, B. Mellado and X. Ruan, *Connecting muon anomalous magnetic moment and multi-lepton anomalies at LHC*, *Chin. Phys. C* **44**(6), 063103 (2020), doi:[10.1088/1674-1137/44/6/063103](https://doi.org/10.1088/1674-1137/44/6/063103), [1909.03969](https://arxiv.org/abs/1909.03969).
- [35] Y. Hernandez, M. Kumar, A. S. Cornell, S.-E. Dahbi, Y. Fang, B. Lieberman, B. Mellado, K. Monnakgotla, X. Ruan and S. Xin, *The anomalous production of multi-lepton and its impact on the measurement of  $Wh$  production at the LHC*, *Eur. Phys. J. C* **81**(4), 365 (2021), doi:[10.1140/epjc/s10052-021-09137-1](https://doi.org/10.1140/epjc/s10052-021-09137-1), [1912.00699](https://arxiv.org/abs/1912.00699).
- [36] S. von Buddenbrock, R. Ruiz and B. Mellado, *Anatomy of inclusive  $t\bar{t}W$  production at hadron colliders*, *Phys. Lett. B* **811**, 135964 (2020), doi:[10.1016/j.physletb.2020.135964](https://doi.org/10.1016/j.physletb.2020.135964), [2009.00032](https://arxiv.org/abs/2009.00032).
- [37] G. Coloretti, A. Crivellin, S. Bhattacharya and B. Mellado, *Searching for low-mass resonances decaying into  $W$  bosons*, *Phys. Rev. D* **108**(3), 035026 (2023), doi:[10.1103/PhysRevD.108.035026](https://doi.org/10.1103/PhysRevD.108.035026), [2302.07276](https://arxiv.org/abs/2302.07276).
- [38] S. Banik, G. Coloretti, A. Crivellin and B. Mellado, *Uncovering New Higgses in the LHC Analyses of Differential  $t\bar{t}$  Cross Sections* (2023), [2308.07953](https://arxiv.org/abs/2308.07953).

- [39] S. von Buddenbrock, N. Chakrabarty, A. S. Cornell, D. Kar, M. Kumar, T. Mandal, B. Mellado, B. Mukhopadhyaya, R. G. Reed and X. Ruan, *Phenomenological signatures of additional scalar bosons at the LHC*, The European Physical Journal C **76**(10) (2016), doi:[10.1140/epjc/s10052-016-4435-8](https://doi.org/10.1140/epjc/s10052-016-4435-8).
- [40] G. Coloretti, A. Crivellin and B. Mellado, *Combined Explanation of LHC Multi-Lepton, Di-Photon and Top-Quark Excesses* (2023), [2312.17314](https://arxiv.org/abs/2312.17314).
- [41] A. Crivellin, Y. Fang, O. Fischer, S. Bhattacharya, M. Kumar, E. Malwa, B. Mellado, N. Rapheeha, X. Ruan and Q. Sha, *Accumulating evidence for the associated production of a new Higgs boson at the LHC*, Phys. Rev. D **108**(11), 115031 (2023), doi:[10.1103/PhysRevD.108.115031](https://doi.org/10.1103/PhysRevD.108.115031), [2109.02650](https://arxiv.org/abs/2109.02650).
- [42] S. Bhattacharya, G. Coloretti, A. Crivellin, S.-E. Dahbi, Y. Fang, M. Kumar and B. Mellado, *Growing Excesses of New Scalars at the Electroweak Scale* (2023), [2306.17209](https://arxiv.org/abs/2306.17209).
- [43] *Search for non-resonant Higgs boson pair production in final states with leptons, taus and photons in pp collisions at  $\sqrt{s} = 13$  TeV with the ATLAS detector*, Tech. rep., CERN, Geneva, All figures including auxiliary figures are available at <https://atlas.web.cern.ch/Atlas/GROUPS/PHYSICS/CONFNOTES/ATLAS-CONF-2024-005> (2024).
- [44] R. Barate *et al.*, *Search for the standard model Higgs boson at LEP*, Phys. Lett. B **565**, 61 (2003), doi:[10.1016/S0370-2693\(03\)00614-2](https://doi.org/10.1016/S0370-2693(03)00614-2), [hep-ex/0306033](https://arxiv.org/abs/hep-ex/0306033).
- [45] *Search for a standard model-like Higgs boson in the mass range between 70 and 110 GeV in the diphoton final state in proton-proton collisions at  $\sqrt{s} = 13$  TeV* (2023).
- [46] *Search for diphoton resonances in the 66 to 110 GeV mass range using  $140 \text{ fb}^{-1}$  of 13 TeV pp collisions collected with the ATLAS detector* (2023).
- [47] A. Tumasyan *et al.*, *Searches for additional Higgs bosons and for vector leptoquarks in  $\tau\tau$  final states in proton-proton collisions at  $\sqrt{s} = 13$  TeV*, JHEP **07**, 073 (2023), doi:[10.1007/JHEP07\(2023\)073](https://doi.org/10.1007/JHEP07(2023)073), [2208.02717](https://arxiv.org/abs/2208.02717).
- [48] G. Aad *et al.*, *Evidence for the Higgs Boson Decay to a Z Boson and a Photon at the LHC*, Phys. Rev. Lett. **132**(2), 021803 (2024), doi:[10.1103/PhysRevLett.132.021803](https://doi.org/10.1103/PhysRevLett.132.021803), [2309.03501](https://arxiv.org/abs/2309.03501).
- [49] M. Aaboud, , G. Aad, B. Abbott, O. Abdinov, B. Abeloos, S. H. Abidi, O. S. AbouZeid, N. L. Abraham, H. Abramowicz, H. Abreu, R. Abreu *et al.*, *Searches for the  $z\gamma$  decay mode of the higgs boson and for new high-mass resonances in pp collisions at  $\sqrt{s} = 13\text{TeV}$  with the ATLAS detector*, Journal of High Energy Physics **2017**(10) (2017), doi:[10.1007/jhep10\(2017\)112](https://doi.org/10.1007/jhep10(2017)112).
- [50] J. Alwall, R. Frederix, S. Frixione, V. Hirschi, F. Maltoni, O. Mattelaer, H.-S. Shao, T. Stelzer, P. Torrielli and M. Zaro, *The automated computation of tree-level and next-to-leading order differential cross sections, and their matching to parton shower simulations*, Journal of High Energy Physics **2014**(7) (2014), doi:[10.1007/jhep07\(2014\)079](https://doi.org/10.1007/jhep07(2014)079).
- [51] T. Sjöstrand, S. Ask, J. R. Christiansen, R. Corke, N. Desai, P. Ilten, S. Mrenna, S. Prestel, C. O. Rasmussen and P. Z. Skands, *An introduction to PYTHIA 8.2*, Computer Physics Communications **191**, 159 (2015), doi:[10.1016/j.cpc.2015.01.024](https://doi.org/10.1016/j.cpc.2015.01.024).
- [52] R. D. Ball *et al.*, *Parton distributions with LHC data*, Nucl. Phys. B **867**, 244 (2013), doi:[10.1016/j.nuclphysb.2012.10.003](https://doi.org/10.1016/j.nuclphysb.2012.10.003), [1207.1303](https://arxiv.org/abs/1207.1303).

- [53] J. de Favereau, C. Delaere, P. Demin, A. Giammanco, V. Lemaître, A. Mertens and M. Selvaggi, *DELPHES 3, A modular framework for fast simulation of a generic collider experiment*, JHEP **02**, 057 (2014), doi:[10.1007/JHEP02\(2014\)057](https://doi.org/10.1007/JHEP02(2014)057), [1307.6346](https://arxiv.org/abs/1307.6346).
- [54] M. Cacciari, G. P. Salam and G. Soyez, *The anti- $k_t$  jet clustering algorithm*, JHEP **04**, 063 (2008), doi:[10.1088/1126-6708/2008/04/063](https://doi.org/10.1088/1126-6708/2008/04/063), [0802.1189](https://arxiv.org/abs/0802.1189).
- [55] M. Cacciari, G. P. Salam and G. Soyez, *FastJet User Manual*, Eur. Phys. J. C **72**, 1896 (2012), doi:[10.1140/epjc/s10052-012-1896-2](https://doi.org/10.1140/epjc/s10052-012-1896-2), [1111.6097](https://arxiv.org/abs/1111.6097).
- [56] L. Vacavant, *b-tagging algorithms and performance in ATLAS*, PoS **2008LHC**, 064 (2008), doi:[10.22323/1.055.0064](https://doi.org/10.22323/1.055.0064).
- [57] J. Albrecht, A. A. Alves, G. Amadio, G. Andronico, N. Anh-Ky, L. Aphecetche, J. Apostolakis, M. Asai, L. Atzori, M. Babik, G. Bagliesi, M. Bandieramonte *et al.*, *A roadmap for HEP software and computing r&d for the 2020s*, Computing and Software for Big Science **3**(1) (2019), doi:[10.1007/s41781-018-0018-8](https://doi.org/10.1007/s41781-018-0018-8).
- [58] A. Ghosh, *Deep generative models for fast shower simulation in ATLAS*, Tech. rep., CERN, Geneva, doi:[10.1088/1742-6596/1525/1/012077](https://doi.org/10.1088/1742-6596/1525/1/012077) (2020).
- [59] S. Otten, S. Caron, W. de Swart, M. van Beekveld, L. Hendriks, C. van Leeuwen, D. Podareanu, R. Ruiz de Austri and R. Verheyen, *Event generation and statistical sampling for physics with deep generative models and a density information buffer*, Nature Communications **12**(1) (2021), doi:[10.1038/s41467-021-22616-z](https://doi.org/10.1038/s41467-021-22616-z).
- [60] J. J. Hodges, *The significance probability of the smirnov two-sample test*, Arkiv fiur Matematik **3**, 469 (1958).
- [61] *Spearman Rank Correlation Coefficient*, pp. 502–505, Springer New York, New York, NY, ISBN 978-0-387-32833-1, doi:[10.1007/978-0-387-32833-1\\_379](https://doi.org/10.1007/978-0-387-32833-1_379) (2008).
- [62] A. Paszke, S. Gross, S. Chintala, G. Chanan, E. Yang, Z. DeVito, Z. Lin, A. Desmaison, L. Antiga and A. Lerer, *Automatic differentiation in pytorch*, In *NIPS-W* (2017).
- [63] S. R. Dubey, S. K. Singh and B. B. Chaudhuri, *Activation functions in deep learning: A comprehensive survey and benchmark*, Neurocomputing **503**, 92 (2022), doi:<https://doi.org/10.1016/j.neucom.2022.06.111>.
- [64] D. P. Kingma and J. Ba, *Adam: A method for stochastic optimization* (2017), [1412.6980](https://arxiv.org/abs/1412.6980).
- [65] R. A. Davis, K.-S. Lii and D. N. Politis, *Remarks on Some Nonparametric Estimates of a Density Function*, Springer New York, New York, NY, ISBN 978-1-4419-8339-8, doi:[10.1007/978-1-4419-8339-8\\_13](https://doi.org/10.1007/978-1-4419-8339-8_13) (2011).
- [66] E. Parzen, *On Estimation of a Probability Density Function and Mode*, The Annals of Mathematical Statistics **33**(3), 1065 (1962), doi:[10.1214/aoms/1177704472](https://doi.org/10.1214/aoms/1177704472).
- [67] K. Cranmer, *Kernel estimation in high-energy physics*, Computer Physics Communications **136**(3), 198 (2001), doi:[https://doi.org/10.1016/S0010-4655\(00\)00243-5](https://doi.org/10.1016/S0010-4655(00)00243-5).
- [68] F. Pedregosa, G. Varoquaux, A. Gramfort, V. Michel, B. Thirion, O. Grisel, M. Blondel, A. Müller, J. Nothman, G. Louppe, P. Prettenhofer, R. Weiss *et al.*, *Scikit-learn: Machine learning in python* (2018), [1201.0490](https://arxiv.org/abs/1201.0490).
- [69] I. Gulrajani, F. Ahmed, M. Arjovsky, V. Dumoulin and A. C. Courville, *Improved training of wasserstein gans*, Advances in neural information processing systems **30** (2017).